Precise determination of two-carrier transport properties in the topological insulator TlBiSe$_2$

G. Eguchi,[1,*] K. Kuroda,[2,†] K. Shirai,[2] Y. Ando,[1] T. Shinjo,[1] A. Kimura,[2] and M. Shiraishi[1]

[1]*Department of Electronic Science and Engineering, Graduate School of Engineering, Kyoto University, Kyoto 615-8510, Japan*
[2]*Graduate School of Science, Hiroshima University, Kagamiyama, Higashi-Hiroshima 739-8526, Japan*

We report the electric transport study of the three-dimensional topological insulator TlBiSe$_2$. We propose an analysis procedure which determines the two-carrier transport properties in precision. Magnetotransport properties reveal a multicarrier conduction of high- and low-mobility electrons in the bulk, which is in qualitative agreement with angle-resolved photoemission results [K. Kuroda *et al.*, Phys. Rev. Lett. **105**, 146801 (2010)]. The temperature dependence of the Hall mobility is explained well with the conventional Bloch-Grüneisen formula and yields the Debye temperature $\Theta_D = 113 \pm 14$ K. The results indicate that the scattering of bulk electrons is dominated by acoustic phonons.

I. INTRODUCTION

Electric and spin transport in three-dimensional (3D) topological insulators has received a great deal of attention because of the insulators' surface Dirac fermions with the unique spin texture. The presence of the spin texture has been confirmed by several experiments employing angle-resolved photoemission spectroscopy (ARPES) and a variety of spin-dependent transport have been proposed [1–8]. In real materials, however, unavoidable bulk conduction often hinders surface conduction.

Electric transport in 3D topological insulators has been analyzed with the so-called two-carrier model, i.e., the parallel conduction of carriers with different mobility [9–11]. Within the model, the resistivity ρ_{xx} in a magnetic field $B = \mu_0 H$ is expressed by

$$\rho_{xx}(B) = \frac{n_1 q_1 \mu_1 + n_2 q_2 \mu_2 + (n_1 q_1 \mu_2 + n_2 q_2 \mu_1)\mu_1\mu_2 B^2}{(n_1 q_1 \mu_1 + n_2 q_2 \mu_2)^2 + (n_1 q_1 + n_2 q_2)^2 \mu_1^2 \mu_2^2 B^2},$$

(1)

where q_1 and q_2, n_1 and n_2, and μ_1 and μ_2 are, respectively, the charges, densities, and mobilities of the carriers. Despite its usability, the model contains four active parameters, which lead to large errors in most cases. The errors have not been discussed and their statistical reliability remains unclear. This is a fundamental issue requiring a more elaborate analysis procedure.

In this article, we report the electric transport of the 3D topological insulator TlBiSe$_2$. The material is known as one of the simplest and most practical materials for transport studies [12–17]. Two-carrier transport properties were determined in precision by applying a procedure proposed in this study. The magnetotransport properties were well explained, accounting for high- and low-mobility electrons in the whole temperature range. The carrier densities were $(0.61 \pm 0.01) \times 10^{19}$ cm^{-3} and $(4.45 \pm 0.01) \times 10^{19}$ cm^{-3}, which were 10^5 times the values expected from the surface. These results indicate that

multicarrier conduction originated from the bulk electrons and the scattering was insensitive to the magnetic field. The temperature dependence of the Hall mobility exhibited a metallic behavior over the whole temperature range and was explained well by the Bloch-Grüneisen formula. This indicates that the scattering of the bulk electrons was dominated by acoustic phonons. It should be noted that the analyses proposed in this article allow a precise identification of the two-carrier transport properties and are therefore useful for all other multicarrier systems.

II. EXPERIMENT

The TlBiSe$_2$ sample used in this study was taken from the same batch in Ref. [16]. As reported in Ref. [16], a significant variation of the chemical composition was revealed between the starting substances and synthesized crystals; the variation resulted in the spontaneous electron doping. The sample, which was synthesized from the starting composition Tl:Bi:Se = 1:1:2 in stoichiometric ratio, corresponded to Tl$_{1-x}$Bi$_{1+x}$Se$_{2-\delta}$ ($x = 0.064, \delta = 0.29$) [16,18]. Electric transport experiments were performed using the conventional six-probe technique down to 2 K with a commercial apparatus (Quantum Design PPMS). Electric contacts were made onto the cleaved surface with room-temperature-cured silver paste under atmospheric conditions. Geometries including the distances of electrodes and the thickness of the sample were determined from optical microscope images. The schematics of the crystal and parallel conduction of the surface and bulk are presented in Figs. 1(a) and 1(b). The optical microscope images are also shown in Fig. 1(c). The sample had a thickness of 0.380 mm. Magnetic fields (maximum strength of ±9 T) were applied parallel to the *c* axis.

III. RESULTS AND ANALYSIS

The temperature dependence of the longitudinal resistivity ρ_{xx} is presented in Fig. 2(a). The inset shows the Hall resistivity ρ_{yx} at 300 and 2 K. The positive temperature coefficient of ρ_{xx} indicates metallic conduction. The negative magnetic coefficients of ρ_{yx} indicate electron conduction. These results are consistent with the ARPES results; the Fermi level was located in the bulk conduction bands [14–16].

———————
*geguchi@kuee.kyoto-u.ac.jp
†Current address: Institute for Solid State Physics, The University of Tokyo, Kashiwanoha 5-1-5, Kashiwa, Chiba 277-8581, Japan.
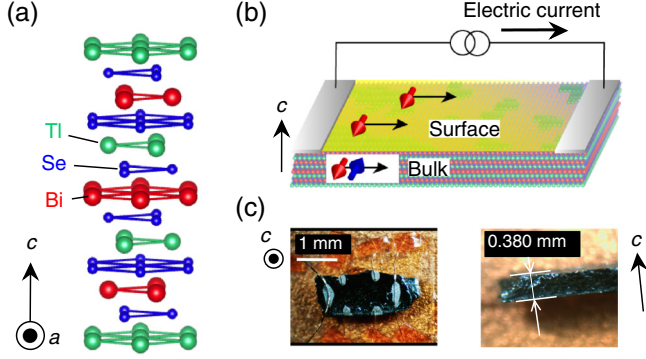
FIG. 1. (Color online) (a) Schematic of the TlBiSe$_2$ crystal with hexagonal coordinates (space group $R\bar{3}m$ [13]). (b) Schematic of parallel conduction of the spin-polarized surface and bulk. The cleaved surface forms thallium islands on the selenium layer [19]. (c) Optical images of the top surface and side surface. The sample thickness was $d = 0.380$ mm.

The ρ_{yx} exhibited a linear magnetic field dependence at each temperature. The temperature dependence of the Hall coefficient $|R_H| = |\rho_{yx}/B|$ and the Hall mobility $\mu_H = |R_H|/\rho_{xx}$ are presented in Fig. 2(b). As shown in the figure, the $|R_H|$ exhibited a small temperature dependence; μ_H also exhibited a temperature variation above 15 K. The $|R_H|$ at 2 K was $(1.775 \pm 0.006) \times 10^{-1}$ cm^3/C and the μ_H at the same temperature was 342 ± 6 cm^2/V s. Because μ_H is in proportion to the scattering time τ, the temperature variation of μ_H is attributed to the temperature dependence of τ. We discuss the dependence later.

The longitudinal resistivity ρ_{xx} exhibited a magnetic field dependence as can be clearly seen in Fig. 3(a). Here $\Delta\rho_{xx}/\rho_{xx} = [\rho_{xx}(B) - \rho_{xx}(0)]/\rho_{xx}(B)$ is the magnetoresistance. For further insight, we transformed the two-carrier model [20]. Within the model, ρ_{xx} is expressed by Eq. (1). Equation (1) was transformed to Eq. (2) using $n_+ = (n_1 + n_2)$, $n_- = (n_1 - n_2)$, $\mu_+ = (\mu_1 + \mu_2)/2$, $\mu_- = (\mu_1 - \mu_2)/2$,
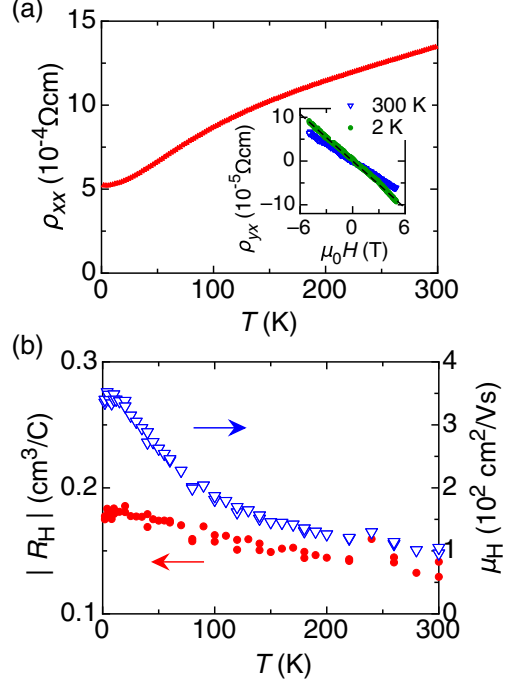

FIG. 2. (Color online) (a) Temperature dependence of the longitudinal resistivity ρ_{xx} in the range 2–300 K. The inset is the Hall resistivity ρ_{yx} at 2 and 300 K. Negative magnetic field dependences indicate electron conduction. A linear fit of ρ_{yx} at 2 K is also presented. (b) Temperature dependence of the Hall coefficient $|R_H| = |\rho_{yx}/\mu_0 H|$ and the Hall mobility $\mu_H = |R_H|/\rho_{xx}$; $|R_H|$ at 2 K was $(1.775 \pm 0.006) \times 10^{-1}$ cm^3/C and μ_H at the same temperature was 342 ± 6 cm^2/V s.

$N = n_-/n_+$, and $M = \mu_-/\mu_+$. In the present case, the charges were $q_1 = q_2 = -e$ and thus $-\mu_+ > 0$ and $-1 \leqslant M \leqslant 1$. We also defined $n_1 \geqslant n_2$, i.e., $0 \leqslant N \leqslant 1$. Finally, $\rho_{xx}(B)$, which was applied in further analyses, was obtained as Eq. (3) and the magnetoresistance was expressed as Eq. (4).

$$\rho_{xx}(B) = \frac{2}{n_+\mu_+}\left[\frac{q_1(1+N)(1+M) + q_2(1-N)(1-M) + [q_1(1+N)(1-M) + q_2(1-N)(1+M)](1-M^2)\mu_+^2 B^2}{[q_1(1+N)(1+M) + q_2(1-N)(1-M)]^2 + [q_1(1+N) + q_2(1-N)]^2(1-M^2)^2\mu_+^2 B^2}\right],$$
(2)

$$\rho_{xx}(B) = \frac{1}{n_+e(-\mu_+)}\left[\frac{1 + NM + (1-M^2)(1-NM)\mu_+^2 B^2}{(1+NM)^2 + (1-M^2)^2\mu_+^2 B^2}\right],$$
(3)

$$\frac{\Delta\rho_{xx}}{\rho_{xx}} = \frac{(1-N^2)M^2(1-M^2)\mu_+^2 B^2}{(1+NM)^2 + (1-N^2M^2)(1-M^2)\mu_+^2 B^2}.$$
(4)

Within the model, R_H and μ_H at $H = 0$, which are presented in Fig. 2(b), are expressed as Eqs. (5) and (6). Using μ_H, Eq. (4) was rewritten as Eq. (7). Because μ_H was an experimental value, $\Delta\rho_{xx}/\rho_{xx}$ is determined by employing two additional parameters N and M. Furthermore, $\rho_{yx}(B)$ was rewritten as Eq. (8) using R_H, μ_H and was thus determined by N and M.

$$R_H = -\frac{1}{n_+e}\left[\frac{1 + 2NM + M^2}{(1+NM)^2}\right],$$
(5)

$$\mu_H = |\mu_+|\left[\frac{1 + 2NM + M^2}{1 + NM}\right],$$
(6)

$$\frac{\Delta\rho_{xx}}{\rho_{xx}} = \frac{(1 - N^2)M^2(1 - M^2)\mu_H^2 B^2}{(1 + 2NM + M^2)^2 + (1 - N^2 M^2)(1 - M^2)\mu_H^2 B^2},$$ (7)

$$\rho_{yx}(B) = R_H \left[\frac{(1 + 2NM + M^2)^3 B + (1 + NM)^2(1 - M^2)^2 \mu_H^2 B^3}{(1 + 2NM + M^2)^3 + (1 + 2NM + M^2)(1 - M^2)^2 \mu_H^2 B^2} \right].$$ (8)

The magnetoresistance $\Delta\rho_{xx}/\rho_{xx}$ at 5 K and the fit with Eq. (7) are presented in Fig. 3(a); the fit yielded $N = 0.76 \pm 0.01$ and $M = -0.586 \pm 0.003$. Also presented are $\Delta\rho_{xx}/\rho_{xx}$ at 300 K and the curve expected from the N and M values with R_H and μ_H at 300 K. The figure shows that the curve at 300 K is consistent with the experiments. Presented in Fig. 3(b) are $\rho_{yx}(B)$ and the curves expected from the same N and M values. The curves also agree well with the experimental results. We thus conclude that the N and M values obtained are invariant within the studied temperature range and the transport properties of the sample are explained well with the two-carrier model.

Once the four parameters of the two-carrier model R_H, μ_H, N, and M were obtained, the densities and mobilities of high- and low-mobility electrons were determined. The densities and the mobilities at 5 K are summarized in Table I. Here $n_1 = n_+(1 + N)/2$, $n_2 = n_+(1 - N)/2$, $\mu_1 = \mu_+(1 + M)$, and $\mu_2 = \mu_+(1 - M)$.

IV. DISCUSSION

As demonstrated above, the magnetotransport properties were well explained by the two-carrier model. We next discuss the origin of these conduction channels with the electronic
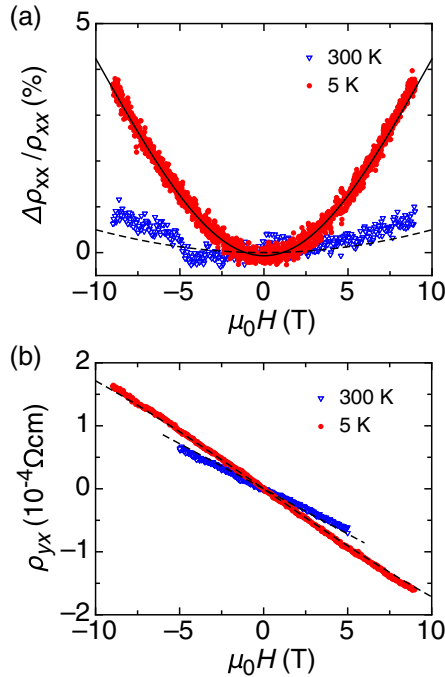

(a)

(b)

FIG. 3. (Color online) (a) Magnetoresistance $\Delta\rho_{xx}/\rho_{xx} = [\rho_{xx}(B) - \rho_{xx}(0)]/\rho_{xx}(B)$ at 300 and 5 K. The fit with Eq. (7) at 5 K is shown by the solid line. The curve expected at 300 K is shown by the dashed line. (b) Hall resistivity ρ_{yx} at 300 and 5 K. The curves expected at each temperature are shown by dashed lines.

band structure. A schematic of the structure revealed by ARPES is presented in Fig. 4 [15,16,21]. The figure shows surface Dirac fermions and two Fermi surfaces of the bulk; one of the Fermi surfaces was around the Γ point and the other around the F point. For the surface Dirac fermions, the two-dimensional carrier density $n_s = k_F^2/4\pi$ was estimated as $\sim 8 \times 10^{12}$ cm^{-2}, where k_F was the Fermi wave number obtained from the ARPES spectrum (Fig. 2 of Ref. [15]). The value of n_s yielded an effective 3D carrier density $n_s/d = 2.1 \times 10^{14}$ cm^{-3}, where $d = 0.380$ mm was the sample thickness. The estimated value of n_s/d was smaller than the experimental values by five orders of magnitude. This indicates that the contribution of the Dirac fermions to ρ_{xx} and ρ_{yx} was negligibly small, i.e., the transport properties are attributed to the bulk electrons. Figure 4 shows that the Fermi surface around the Γ point has a larger Fermi cross section and a larger band mass than that around the F point. These band characters are consistent with the two-carrier model, where the Fermi surface around the Γ point yields higher carrier density and lower mobility, i.e., n_1 and μ_1. It is also concluded that the minor electrons with carrier density n_2 and mobility μ_2 can be attributed to the Fermi surface around the F point.

As discussed above, surface transport is hidden in bulk metallic conduction with carrier density $\sim 10^{19}$ cm^{-3}. In contrast, a bulk insulating state with carrier density $< 10^{17}$ cm^{-3} was demonstrated for Tl$_{1-x}$Bi$_{1+x}$Se$_{2-\delta}$ ($x \leqslant 0.028, \delta = 0.28$) and the surface metallic conduction was distinguished [16,17]. These results indicate the presence of a metal-insulator transition in bulk between $x = 0.064$ and 0.028 and surface transport can be distinguished only in the bulk insulating samples.

Finally, we discuss the temperature dependence of scattering realized in the system. The scattering time is in proportion to the mobility and the temperature dependence of μ_+ is thus attributed to the temperature dependence of the average scattering time τ. Note that the agreement with the two-carrier model indicates that the scattering was insensitive to the magnetic field. As discussed above, the temperature dependences of N and M were negligibly small. These results indicate that μ_H can be expressed as $\mu_H = 0.816|\mu_+|$ using the N and M values obtained [see Eq. (6)] and that the temperature dependence of μ_H can be attributed to τ. The temperature dependence of μ_H^{-1} is presented in Fig. 5. The fit

TABLE I. Electric transport properties at 5 K obtained from the two-carrier model. Here n_1 and n_2, and μ_1 and μ_2 are, respectively, the densities and mobilities of the electrons.

n_1	$(4.45 \pm 0.01) \times 10^{19}$ cm^{-3}
n_2	$(0.61 \pm 0.01) \times 10^{19}$ cm^{-3}
μ_1	176 ± 2 cm^2/V s
μ_2	676 ± 2 cm^2/V s

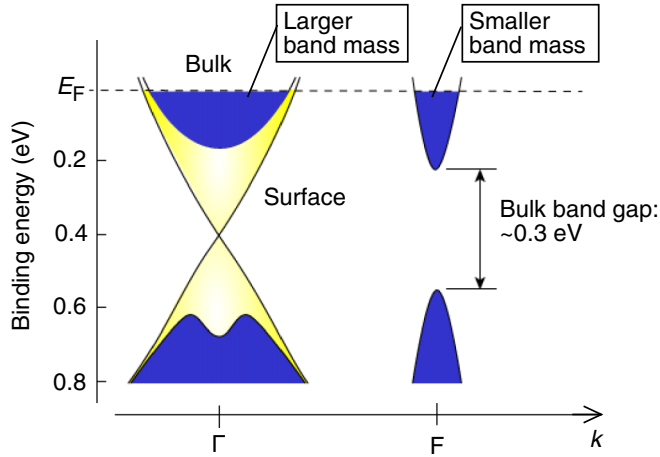FIG. 4. (Color online) Schematic of the energy band dispersion of TlBiSe$_2$ revealed by ARPES [15,16,21]. The smaller band curvature around the Γ point results in a larger band mass of electrons. The larger band curvature around the F point results in smaller band mass. The amplitude of the minimum bulk band gap is also presented.

with the Bloch-Grüneisen formula

$$\frac{1}{\tau} \propto \left(\frac{T^5}{\Theta_D^6}\right) \int_0^{\Theta_D/T} \frac{x^5}{(e^x - 1)(1 - e^{-x})} dx, \qquad (9)$$

which describes the temperature dependence of acoustic phonon scattering, is also presented. Here Θ_D is the Debye temperature determined in the present transport experiment. As shown in Fig. 5, the temperature dependence of $1/\mu_H \propto 1/\tau$ agrees well with the formula, which yields $\Theta_D = 113 \pm 14$ K. Note that Θ_D agrees with the Debye temperature determined from the specific heat [22]. The result indicates that the scattering was dominated by acoustic phonons. Similar results are often seen for metals of a weakly correlated electron system, indicating that the scattering of bulk electrons is explained by the conventional theory of metals.

V. CONCLUSION

We investigated the transport properties of the 3D topological insulator TlBiSe$_2$. Two-carrier transport properties
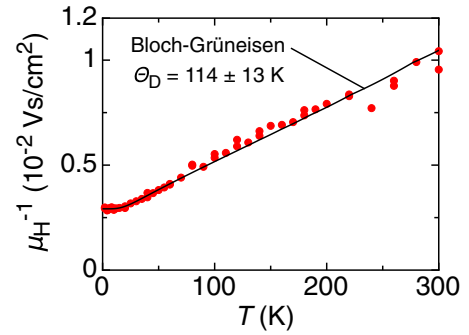

FIG. 5. (Color online) Temperature dependence of the inverse Hall mobility μ_H^{-1}. The fit with the Bloch-Grüneisen formula yields the Debye temperature $\Theta_D = 114 \pm 13$ K. See the text for details.

were determined in precision. The magnetotransport properties were well explained, accounting for high- and low-mobility electrons in the whole temperature range. This indicated that the scattering of electrons was insensitive to the magnetic field. The transport properties obtained were consistent with ARPES results and contributions of the surface transport were negligibly small over the entire temperature range studied. The scattering of bulk electrons was dominated by acoustic phonons. The results indicate that the bulk transport properties of the TlBiSe$_2$ sample were in the vicinity of those of conventional metals. The simple nature of bulk conduction hints at the proper verification of surface transport properties. It should be emphasized that the analysis using the conventional two-carrier model with four active parameters leads to large errors. Instead, the analysis proposed in this study exhibited sufficiently small errors and therefore possessed statistical reliability. We also note that the procedure should be useful for all other transport studies.

[1] M. Hasan and C. Kane, Rev. Mod. Phys. **82**, 3045 (2010).

[2] X.-L. Qi and S.-C. Zhang, Rev. Mod. Phys. **83**, 1057 (2011).

[3] Y. Ando, J. Phys. Soc. Jpn. **82**, 102001 (2013).

[4] Z.-H. Pan, E. Vescovo, A. V. Fedorov, D. Gardner, Y. S. Lee, S. Chu, G. D. Gu, and T. Valla, Phys. Rev. Lett. **106**, 257004 (2011).

[5] C. H. Li, O. M. J. van 't Erve, J. T. Robinson, Y. Liu, L. Li, and B. T. Jonker, Nat. Nanotechnol. **9**, 218 (2014).

[6] J. Tang, L.-T. Chang, X. Kou, K. Murata, E. S. Choi, M. Lang, Y. Fan, Y. Jiang, M. Montazeri, W. Jiang, Y. Wang, L. He, and K. L. Wang, Nano Lett. **14**, 5423 (2014).

[7] Y. Ando, T. Hamasaki, T. Kurokawa, K. Ichiba, F. Yang, M. Novak, S. Sasaki, K. Segawa, Y. Ando, and M. Shiraishi, Nano Lett. **14**, 6226 (2014).

[8] D. Culcer, E. H. Hwang, T. D. Stanescu, and S. Das Sarma, Phys. Rev. B **82**, 155457 (2010).

[9] Z. Ren, A. A. Taskin, S. Sasaki, K. Segawa, and Y. Ando, Phys. Rev. B **82**, 241306 (2010).

[10] A. A. Taskin, Z. Ren, S. Sasaki, K. Segawa, and Y. Ando, Phys. Rev. Lett. **107**, 016801 (2011).

[11] N. Bansal, Y. S. Kim, M. Brahlek, E. Edrey, and S. Oh, Phys. Rev. Lett. **109**, 116804 (2012).

[12] B. Yan, C.-X. Liu, H.-J. Zhang, C.-Y. Yam, X.-L. Qi, T. Frauenheim, and S.-C. Zhang, Europhys. Lett. **90**, 37002 (2010).

[13] H. Lin, R. S. Markiewicz, L. A. Wray, L. Fu, M. Z. Hasan, and A. Bansil, Phys. Rev. Lett. **105**, 036404 (2010).

[14] T. Sato, K. Segawa, H. Guo, K. Sugawara, S. Souma, T. Takahashi, and Y. Ando, Phys. Rev. Lett. **105**, 136802 (2010).

[15] K. Kuroda, M. Ye, A. Kimura, S. V. Eremeev, E. E. Krasovskii, E. V. Chulkov, Y. Ueda, K. Miyamoto, T. Okuda, K. Shimada, H. Namatame, and M. Taniguchi, Phys. Rev. Lett. **105**, 146801 (2010).

[16] K. Kuroda, G. Eguchi, K. Shirai, M. Shiraishi, M. Ye, K. Miyamoto, T. Okuda, S. Ueda, M. Arita, H. Namatame, M. Taniguchi, Y. Ueda, and A. Kimura, Phys. Rev. B **91**, 205306 (2015).

[17] G. Eguchi, K. Kuroda, K. Shirai, A. Kimura, and M. Shiraishi, Phys. Rev. B **90**, 201307 (2014).

[18] Samples of our preceding studies [15,19] were also synthesized from the same starting composition Tl:Bi:Se = 1:1:2, thus expected to be $Tl_{1-x}Bi_{1+x}Se_{2-\delta}$ ($x = 0.064, \delta = 0.29$).

[19] K. Kuroda, M. Ye, E. F. Schwier, M. Nurmamat, K. Shirai, M. Nakatake, S. Ueda, K. Miyamoto, T. Okuda, H. Namatame, M. Taniguchi, Y. Ueda, and A. Kimura, Phys. Rev. B **88**, 245308 (2013).

[20] N. W. Ashcroft and N. D. Mermin, *Solid State Physics*, 1st ed. (Brooks/Cole, Pacific Grove, 1976).

[21] The Fermi level of the $Tl_{1-x}Bi_{1+x}Se_{2-\delta}$ ($x = 0.064$, $\delta = 0.29$), reported in Ref. [16], was almost identical to that of Ref. [15]. Therefore, a wide-range mapping of the ARPES presented in Fig. 3 in Ref. [15] represents the band structure of the sample.

[22] V. Bazakutsa, M. Vasil'eva, V. Ustimenko, and L. Mokhir, J. Eng. Phys. **37**, 1191 (1979).